Supporting Information

Kragelj et al. 10.1073/pnas.1419528112

SI Materials and Methods

Expression and Purification of the Regulatory Domain of MKK7. Regions of the intrinsically disordered regulatory domain of MKK7 comprising one (residues 1–42), two (residues 1–55), or three docking sites (residues 1–100) were subcloned into a modified pET-28a vector containing an N-terminal thioredoxin and a 6xHis tag followed by a tobacco etch virus (TEV) cleavage site. *Escherichia coli* BL21(DE3) cells transformed with one of the MKK7 constructs were grown in LB medium at 37 °C until the optical density (OD) at 600 nm reached 0.6. Protein expression was induced by addition of isopropyl β-D-thiogalactopyranoside (IPTG) to a final concentration of 1 mM. The cultures were grown while shaking at 37 °C for an additional 3 h. The cells were harvested by centrifugation and frozen at −80 °C. Isotopically $^{15}N/^{13}C$- and ^{15}N-labeled samples were produced by growing transformed *E. coli* BL21(DE3) cells according to the protocol described by Marley et al. (1).

All constructs were purified by using Ni affinity chromatography followed by size-exclusion chromatography. For cell lysis, inhibitor mixture (Roche) was added to the purification buffer (50 mM Hepes pH 8.0, 150 mM NaCl, 5 mM imidazole, 5 mM β-mercaptoethanol). The elution buffer was the same as the purification buffer, but with 250 mM imidazole. After removing thioredoxin and the 6xHis tag with TEV protease and after a second Ni affinity column, size-exclusion chromatography was performed on a Superdex 75 column (GE Healthcare) equilibrated with NMR buffer [50 mM Hepes pH 7.0, 150 mM NaCl, 5% (vol/vol) glycerol, 2 mM DTT] or ITC buffer [50 mM Hepes pH 8.2, 150 mM NaCl, 10% (vol/vol) glycerol, 0.5 mM TCEP].

Expression and Purification of Full-Length MKK7. Synthetic codon-optimized full-length MKK7-β1 gene was subcloned into a pET vector with an N-terminal 6xHis tag followed by a TEV cleavage site. Transformed *E. coli* BL21(DE3) cells were initially grown in LB medium at 37 °C and were transferred to 18 °C when the OD at 600 nm reached 0.3. Protein expression was induced with addition of IPTG at OD_{600} of 0.6. Cells were harvested 12–14 h later by centrifugation and were frozen at −80 °C.

Harvested cells were resuspended in lysis buffer [50 mM Hepes pH 8.0, 150 mM NaCl, 10% (vol/vol) glycerol, 5 mM imidazol, 5 mM β-mercaptoethanol, protease inhibitor mixture (Roche)], sonicated on ice, applied to Ni affinity chromatography column, and washed with lysis buffer without protease inhibitor mixture. Protein was eluted with elution buffer (50 mM Hepes pH 8.0, 150 mM NaCl, 250 mM imidazol, 5 mM β-mercaptoethanol) by using a gradient elution one column volume long.

The protein was diluted to 1 mg/mL and dialyzed against NMR buffer. The protein was concentrated and purified on a size-exclusion chromatography column equilibrated with NMR buffer. Under these conditions, the protein concentrates to 70 μM. All purification steps were performed at 4 °C.

Expression and Purification of JNK1. Synthetic codon-optimized JNK1α1 gene corresponding to residues 1–364 was subcloned into a pET vector with a C-terminal 6xHis tag. Transformed *Escherichia coli* BL21(DE3) cells were initially grown in LB medium at 37 °C and were transferred to 18 °C when the OD at 600 nm reached 0.3. Protein expression was induced with addition of IPTG at OD_{600} of 0.6. Cells were harvested 12–14 h later by centrifugation and were frozen at −80 °C.

Harvested cells were resuspended in lysis buffer [50 mM Hepes pH 8.0, 150 mM NaCl, 10% (vol/vol) glycerol, 5 mM imidazole, 5 mM β-mercaptoethanol, protease inhibitor mixture (Roche)], sonicated on ice, applied to Ni affinity chromatography column, and washed with lysis buffer without protease inhibitor mixture. Protein was eluted with elution buffer (50 mM Hepes pH 8.0, 150 mM NaCl, 250 mM imidazole, 5 mM β-mercaptoethanol) by using a gradient elution one column volume long.

For ITC measurements, the protein was loaded on a size-exclusion chromatography column equilibrated with ITC buffer. Protein concentrated to 100 μM under these conditions. For NMR measurements, the protein was diluted to 0.5 mg/mL and dialyzed against NMR buffer. The protein was concentrated and subsequently purified on a size-exclusion chromatography column equilibrated with NMR buffer. Under these conditions, the protein concentrates to ∼60 μM. All purification steps were performed at 4 °C.

Isothermal Titration Calorimetry. ITC measurements were performed on the MicroCal iTC200 (GE Healthcare) at 20 °C. Injection parameters were identical for all experiments (1.5 μL injections every 180 s, 26 in total at a stirring speed of 800 rpm). Before the experiments, a size-exclusion chromatography was performed for all proteins by using the ITC buffer [50 mM Hepes pH 8.2, 150 mM NaCl, 10% (vol/vol) glycerol, 0.5 mM TCEP]. Constructs of the regulatory domain of MKK7 were titrated into a solution of JNK1 with concentrations between 45 μM and 90 μM. For the constructs of the intrinsically disordered domain of MKK7, the Trx 6xHis tag was not removed by the TEV protease, allowing accurate concentrations to be determined from UV absorbance and calculated molar extinction coefficients. A control experiment was carried out, showing that no interaction occurs between isolated Trx and JNK1. The analysis of the ITC titration data revealed a systematic overestimation of the JNK1 concentrations and we, therefore, corrected all of the JNK1 concentrations by the same factor (70%) before the fitting of the experimental data.

Peptides (>98% purity) corresponding to the three docking sites of MKK7 (ARRRIDLNLDIS, QRPRPTLQLPLA, and ARPRHMLGLP) were obtained from CASLO Laboratory ApS (Denmark). The peptide corresponding to the first docking site D1 was not soluble and could, therefore, not be used for affinity measurements. The concentrations of the peptides corresponding to the docking sites D2 and D3 were estimated by amino acid analysis.

Spectral Assignment and RDC Measurements. Spectral assignments of the regulatory domain of MKK7 (residues 1–100) were obtained at 5 °C, 150 mM NaCl, 50 mM Hepes, pH 7.0 by using a set of BEST-type triple resonance spectra: HNCO, intraresidue HN(CA)CO, HN(CO)CA, intraresidue HNCA, HN(COCA)CB, and intraresidue HN(CA)CB (2). All spectra were processed in NMRPipe (3), and the program MARS (4) was used for automatic assignment of spin systems followed by manual verification. Random coil values for the calculation of secondary chemical shifts were obtained from the neighbor corrected intrinsically disordered protein library (5).

RDCs were obtained at 5 °C by aligning the regulatory domain of MKK7 in a liquid crystal composed of poly-ethylene glycol (PEG C8E5, Sigma) and 1-octanol, giving rise to a ^2H quadrupole splitting of 31 Hz (6). The RDCs were measured by using BEST-type 3D HNCO- and HN(CO)CA experiments modified to allow for spin-coupling measurements in the ^{13}C dimension (7).

Ensemble Description of MKK7. Ensembles of the regulatory domain of MKK7 were constructed by using Flexible-Meccano (8, 9) imposing α-helices of different lengths and different positions within the region comprising residues 3–32 (minimum helix length was four amino acids). A total of 378 ensembles comprising 10,000 conformers each were created, and ensemble-averaged chemical shifts and RDCs were calculated by using SPARTA (10) and PALES (11), respectively. In addition, a statistical coil ensemble comprising 50,000 conformers was used to obtain expected chemical shifts and RDCs for MKK7 in the absence of any helical elements. The genetic algorithm ASTEROIDS was used to select combinations of ensembles that best fit the experimental data i.e., a limited number of helical ensembles in exchange with the unfolded form as described (12, 13). Three different types of RDCs, $^1D_{NH}$, $^1D_{C\alpha H\alpha}$, and $^1D_{C\alpha C'}$, were used in the optimization procedure together with Cα chemical shifts for the residues 1–35. The RDCs mainly report on the capping of specific helices, whereas the Cα chemical shifts report on the population of these helices. We decided to use only the chemical shift type that is the most sensitive to helical population in this step, in order not to introduce any bias from other chemical shift types that are less sensitive to helical populations. The data were included with experimental uncertainties of 1.0 Hz ($^1D_{NH}$), 2.0 Hz ($^1D_{C\alpha H\alpha}$), and 0.3 Hz ($^1D_{C\alpha C'}$) and 0.15 ppm (Cα chemical shifts), ensuring an almost equal contribution to the total target function. The number of helical ensembles, n, was gradually increased (from $n = 1$ to $n = 4$) and a standard F test was applied to the reproduction of the RDCs at each step to test for the statistical significance of adding additional helical ensembles to the fitting procedure ($n = 2$: $P < 0.0001$, $n = 3$: $P = 0.0005$, $n = 4$: $P = 0.2610$). The analysis shows that residues 1–35 of MKK7 is best described by an ensemble of three specific helical conformers in exchange with an unfolded form.

In a second step, we carried out an ensemble selection of the entire regulatory domain on the basis of the experimental chemical shifts and RDCs. Five ensembles comprising 200 conformers each were selected from a large pool of structures containing the already described conformational helical equilibrium at the N terminus. This approach provides a way of imposing cooperative helical elements in the final ensemble selections. Available experimental data ($^{13}C\alpha$, $^{13}C\beta$, $^{13}C'$, ^{15}N, and $^1H^N$ chemical shifts and $^1D_{NH}$, $^1D_{C\alpha H\alpha}$, and $^1D_{C\alpha C'}$ RDCs) were used in the ensemble selection by using the following experimental uncertainties: 0.5 Hz ($^1D_{NH}$), 1.0 Hz ($^1D_{C\alpha H\alpha}$), 0.15 Hz ($^1D_{C\alpha C'}$), 0.1 ppm ($^{13}C\alpha$, $^{13}C\beta$, $^{13}C'$), 0.2 ppm (^{15}N), and 0.04 ppm ($^1H^N$). The $^4D_{HNH\alpha}$ couplings were retained for cross-validation. In general, the protocol for the ensemble selections used five iteration steps (regeneration of pool and subsequent selections) as described (14, 15). A representative ensemble of MKK7 has been deposited in the protein ensemble database (pE-DB) (16) under accession no. PED5AAB. Pearson correlation coefficients (R) and rmsd values were calculated for the reproduction of each dataset by the ASTEROIDS ensembles: $^1D_{NH}$ ($R = 0.98$, rmsd = 2.06 Hz), $^1D_{C\alpha H\alpha}$ ($R = 0.86$, rmsd = 3.63 Hz), $^1D_{C\alpha C'}$ ($R = 0.81$, rmsd = 0.55 Hz), $^4D_{HNH\alpha}$ ($R = 0.82$, rmsd = 4.81 Hz, passive dataset), $^{13}C\alpha$ ($R = 0.95$, rmsd = 0.23 ppm), $^{13}C\beta$ ($R = 0.82$, rmsd = 0.21 ppm), $^{13}C'$ ($R = 0.91$, rmsd = 0.36 ppm), ^{15}N ($R = 0.84$, rmsd = 0.62 ppm), and $^1H^N$ ($R = 0.75$, rmsd = 0.09 ppm).

NMR Titration of MKK7 with JNK1. The ^{15}N-labeled regulatory domain of MKK7 was titrated with unlabeled JNK1 and ^1H-^{15}N HSQC spectra were recorded for each titration step for the following concentrations (μM) of MKK7:JNK1: 84:0.0 (0%), 84:6.9 (8%), 84:11.7 (14%), 84:23.4 (28%), 84:40.7 (49%), 84:58.0 (69%), and 42:70.5 (168%). The titration was carried out at 5 °C in a buffer consisting of 150 mM NaCl, 50 mM Hepes, pH 7.0 containing 5% (vol/vol) glycerol. The intensity ratio I/I^0 is calculated, where I is the intensity in the spectrum with a given molar ratio of JNK1, whereas I^0 is the intensity in the spectrum without JNK1. In addition to the HSQC spectra, ^{15}N R_2 (CPMG) relaxation experiments were recorded at a ^1H frequency of 600 MHz for the samples with the following molar ratios of JNK1/MKK7: 0%, 14%, and 28%. The R_2 rates were recorded by using a standard pulse sequence (17) with the decay of the magnetization sampled at the following time points: 70, 130, 10, 90, 250, 30, 210, 50, 170, and 70 ms. The delay at 70 ms was repeated for the purpose of error estimation.

In addition to the titration at 5 °C, we also obtained ^1H-^{15}N HSQC spectra and $R_{1\rho}$ relaxation rates (spin lock field of 1.5 kHz) of the regulatory domain at 20 °C in the absence and presence of JNK1. The following concentrations (micromolar) were used of MKK7:JNK1: 155:0.0 (0%), 155:23.3 (15%), 155:46.5 (30%).

We also obtained ^1H-^{15}N HSQC spectra at 5 °C of a shorter construct of MKK7 (residues 1–42) containing only the D1 docking site. The HSQC spectra were recorded in the absence and in presence of JNK1 (20% molar ratio).

Relaxation Dispersion and Chemical Exchange Saturation Transfer Experiments. The ^{15}N relaxation dispersion (18) and CEST experiments (19) were carried out on a ^{13}C, ^{15}N-labeled sample of the regulatory domain of MKK7 (200 μM) containing 10% molar ratio of JNK1. All experiments were recorded at 5 °C in a buffer consisting of 150 mM NaCl, 50 mM Hepes, pH 7.0 containing 5% (vol/vol) glycerol. The relaxation dispersion experiments were carried out at ^1H frequencies of 600 and 800 MHz by using a constant-time relaxation delay of 32 ms. Fourteen points (including two duplicates) were recorded for each dispersion curve corresponding to CPMG frequencies between 31.25 and 1,000 Hz. Using the same parameters, relaxation dispersion was also recorded in free MKK7 at 800 MHz and 5 °C.

The CEST experiments were carried out at a ^1H frequency of 700 MHz with two different ^{15}N B_1 field strengths of 22 and 44.5 Hz, where the B_1 field was applied during a constant period of 0.3 s. The experiments were recorded with 78 (B_1 field of 44.5 Hz) or 94 (B_1 field of 22 Hz) 2D planes with the position of the ^{15}N B_1 field ranging from 101.2 to 130.6 ppm in steps of 30 Hz (B_1 field of 44.5 Hz) or 25 Hz (B_1 field of 25 Hz). The relaxation dispersion and CEST data were fitted by using ChemEx (19) assuming a two-site exchange model. For the D2 docking site, the residues were fitted individually, whereas for the D3 docking site, all residues were fitted simultaneously to a single exchange rate and population as described in the text. For the D3 docking site, it was not necessary to evoke a ΔR_2 contribution to fit the experimental CEST profiles and they were therefore fixed to 0 for all residues.

NMR of Full-Length MKK7. The ^1H-^{15}N HSQC spectrum of full-length MKK7 (68 μM) was recorded at 25 °C in a buffer consisting of 150 mM NaCl, 50 mM Hepes, and 5% (vol/vol) glycerol at pH 7.0. To compare this spectrum with that of the isolated regulatory domain, a ^1H-^{15}N HSQC spectrum was recorded of the regulatory domain under identical conditions. The spectral assignment obtained at 5 °C was transferred to the spectrum at 25 °C by using a HSQC temperature titration.

Full-length ^{15}N-labeled MKK7 was titrated with unlabeled JNK1 and ^1H-^{15}N HSQC spectra were recorded for each titration step for the following concentrations (micromolar) of MKK7:JNK1: 68:0 (0%), 51:10 (20%) and 38:15 (40%). The titration was carried out at 25 °C in a buffer consisting of 150 mM NaCl and 50 mM Hepes, pH 7.0 containing 5% (vol/vol) glycerol.

Crystal Structure of JNK1 in Complex with D2 Peptide. The complex between JNK1 and the peptide (QRPRPTLQLPLA) corresponding to the second docking site of MKK7 crystallized in space group C2 with unit cell parameters of $a = 108.4$, $b = 179.6$, $c = 100.8$,

$\beta = 110.2$ with four molecules of JNK1 and four peptides in the asymmetric unit.

Oscillation data were collected on the ESRF beamline ID29 (20) at 0.9763 Å wavelength on a Pilatus 6M-F detector with 37-ms exposures and 0.15 degrees per frame. Data were processed with XDS/XSCALE (21), and a free set of 3,985 (5%) reflections was selected in thin shells and set aside. Phases were obtained by molecular replacement with PHASER (22), splitting the search model (3O2M) into two subdomains consisting of residues 7–110 + 334–364, and 111–333. Solutions were found for the first subdomain with translational Z scores of 34.8, 34.2, 28.8, and 28.8 and for the second domain with translational Z scores of 26.4, 46.1, 54.8, and 50.1. The structures were refined by multiple rounds of manual rebuilding in COOT (23) followed by refinement in BUSTER (24). Several regions of poor electron density were left unmodeled, specifically the loops in regions K30-I39, G177-P184, P281-L289, and the linker region between P338 and the C-terminal helix. The latter region is especially poorly ordered in subunit B. The structure refined to acceptable geometry and R values (Table S1), but the overall Wilson B factor and average B values are higher than other structures at the same resolution. The structure was deposited in the PDB database under accession no. 4UX9.

1. Marley J, Lu M, Bracken C (2001) A method for efficient isotopic labeling of recombinant proteins. *J Biomol NMR* 20(1):71–75.
2. Lescop E, Schanda P, Brutscher B (2007) A set of BEST triple-resonance experiments for time-optimized protein resonance assignment. *J Magn Reson* 187(1):163–169.
3. Delaglio F, et al. (1995) NMRPipe: A multidimensional spectral processing system based on UNIX pipes. *J Biomol NMR* 6(3):277–293.
4. Jung Y-S, Zweckstetter M (2004) Mars — robust automatic backbone assignment of proteins. *J Biomol NMR* 30(1):11–23.
5. Tamiola K, Acar B, Mulder FAA (2010) Sequence-specific random coil chemical shifts of intrinsically disordered proteins. *J Am Chem Soc* 132(51):18000–18003.
6. Rückert M, Otting G (2000) Alignment of biological macromolecules in novel nonionic liquid crystalline media for NMR experiments. *J Am Chem Soc* 122(32):7793–7797.
7. Rasia RM, Lescop E, Palatnik JF, Boisbouvier J, Brutscher B (2011) Rapid measurement of residual dipolar couplings for fast fold elucidation of proteins. *J Biomol NMR* 51(3): 369–378.
8. Bernadó P, et al. (2005) A structural model for unfolded proteins from residual dipolar couplings and small-angle x-ray scattering. *Proc Natl Acad Sci USA* 102(47): 17002–17007.
9. Ozenne V, et al. (2012) Flexible-meccano: A tool for the generation of explicit ensemble descriptions of intrinsically disordered proteins and their associated experimental observables. *Bioinformatics* 28(11):1463–1470.
10. Shen Y, Bax A (2007) Protein backbone chemical shifts predicted from searching a database for torsion angle and sequence homology. *J Biomol NMR* 38(4):289–302.
11. Zweckstetter M, Bax A (2000) Prediction of sterically induced alignment in a dilute liquid crystalline phase: Aid to protein structure determination by NMR. *J Am Chem Soc* 122(15):3791–3792.
12. Jensen MR, et al. (2008) Quantitative conformational analysis of partially folded proteins from residual dipolar couplings: Application to the molecular recognition element of Sendai virus nucleoprotein. *J Am Chem Soc* 130(25):8055–8061.
13. Jensen MR, et al. (2011) Intrinsic disorder in measles virus nucleocapsids. *Proc Natl Acad Sci USA* 108(24):9839–9844.
14. Jensen MR, Salmon L, Nodet G, Blackledge M (2010) Defining conformational ensembles of intrinsically disordered and partially folded proteins directly from chemical shifts. *J Am Chem Soc* 132(4):1270–1272.
15. Ozenne V, et al. (2012) Mapping the potential energy landscape of intrinsically disordered proteins at amino acid resolution. *J Am Chem Soc* 134(36):15138–15148.
16. Varadi M, et al. (2014) pE-DB: A database of structural ensembles of intrinsically disordered and of unfolded proteins. *Nucleic Acids Res* 42(Database issue):D326–D335.
17. Farrow NA, et al. (1994) Backbone dynamics of a free and phosphopeptide-complexed Src homology 2 domain studied by 15N NMR relaxation. *Biochemistry* 33(19): 5984–6003.
18. Hansen DF, Vallurupalli P, Kay LE (2008) An improved 15N relaxation dispersion experiment for the measurement of millisecond time-scale dynamics in proteins. *J Phys Chem B* 112(19):5898–5904.
19. Vallurupalli P, Bouvignies G, Kay LE (2012) Studying "invisible" excited protein states in slow exchange with a major state conformation. *J Am Chem Soc* 134(19): 8148–8161.
20. de Sanctis D, et al. (2012) ID29: A high-intensity highly automated ESRF beamline for macromolecular crystallography experiments exploiting anomalous scattering. *J Synchrotron Radiat* 19(Pt 3):455–461.
21. Kabsch W (2010) XDS. *Acta Crystallogr D Biol Crystallogr* 66(Pt 2):125–132.
22. McCoy AJ, et al. (2007) Phaser crystallographic software. *J Appl Cryst* 40(Pt 4):658–674.
23. Emsley P, Cowtan K (2004) Coot: Model-building tools for molecular graphics. *Acta Crystallogr D Biol Crystallogr* 60(Pt 12 Pt 1):2126–2132.
24. Bricogne G, et al. (2011) *BUSTER version 1.10.0* (Global Phasing Ltd., Cambridge, UK).

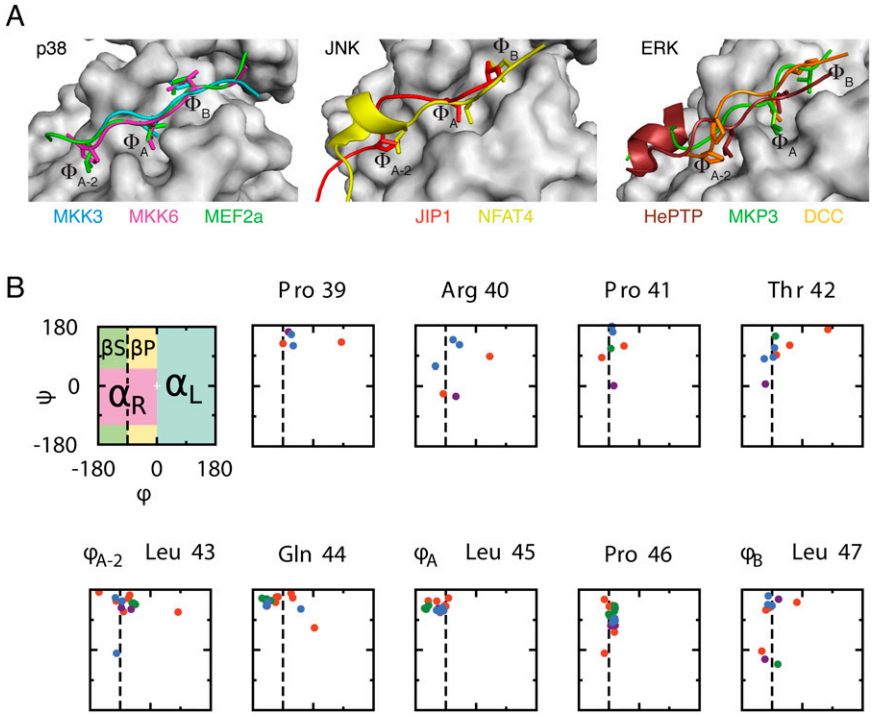

Fig. S1. Conformations of docking site peptides in crystal structures. (*A*) Crystal structures of p38, JNK, and ERK in complex with different docking site peptides. The following crystal structures were used as follows: p38:MKK3 (1LEZ) (1), p38:MKK6 (2Y8O) (2), p38:MEF2A (1LEW) (1), JNK:JIP1 (2G01) (3), JNK:NFAT4 (2XRW) (2), ERK:HePTP (2GPH) (4), ERK:MKP3 (2FYS) (5), and ERK:DCC (3O71) (6). (*B*) Analysis of dihedral angle distributions in docking site peptides obtained from crystal structures of the peptides in complex with ERK, p38, and JNK. Dihedral angles are shown of p38 and ERK docking site peptides (orange) and three different JNK docking site peptides JIP1 (green), NFAT4 (magenta), and MKK7 (blue).

1. Chang CI, Xu BE, Akella R, Cobb MH, Goldsmith EJ (2002) Crystal structures of MAP kinase p38 complexed to the docking sites on its nuclear substrate MEF2A and activator MKK3b. *Mol Cell* 9(6):1241–1249.
2. Garai Á, et al. (2012) Specificity of linear motifs that bind to a common mitogen-activated protein kinase docking groove. *Sci Signal* 5(245):ra74.
3. Hom RK, et al. (2010) Design and synthesis of disubstituted thiophene and thiazole based inhibitors of JNK. *Bioorg Med Chem Lett* 20(24):7303–7307.
4. Zhou T, Sun L, Humphreys J, Goldsmith EJ (2006) Docking interactions induce exposure of activation loop in the MAP kinase ERK2. *Structure* 14(6):1011–1019.
5. Liu S, Sun J-P, Zhou B, Zhang Z-Y (2006) Structural basis of docking interactions between ERK2 and MAP kinase phosphatase 3. *Proc Natl Acad Sci USA* 103(14):5326–5331.
6. Ma W, et al. (2010) Phosphorylation of DCC by ERK2 is facilitated by direct docking of the receptor P1 domain to the kinase. *Structure* 18(11):1502–1511.

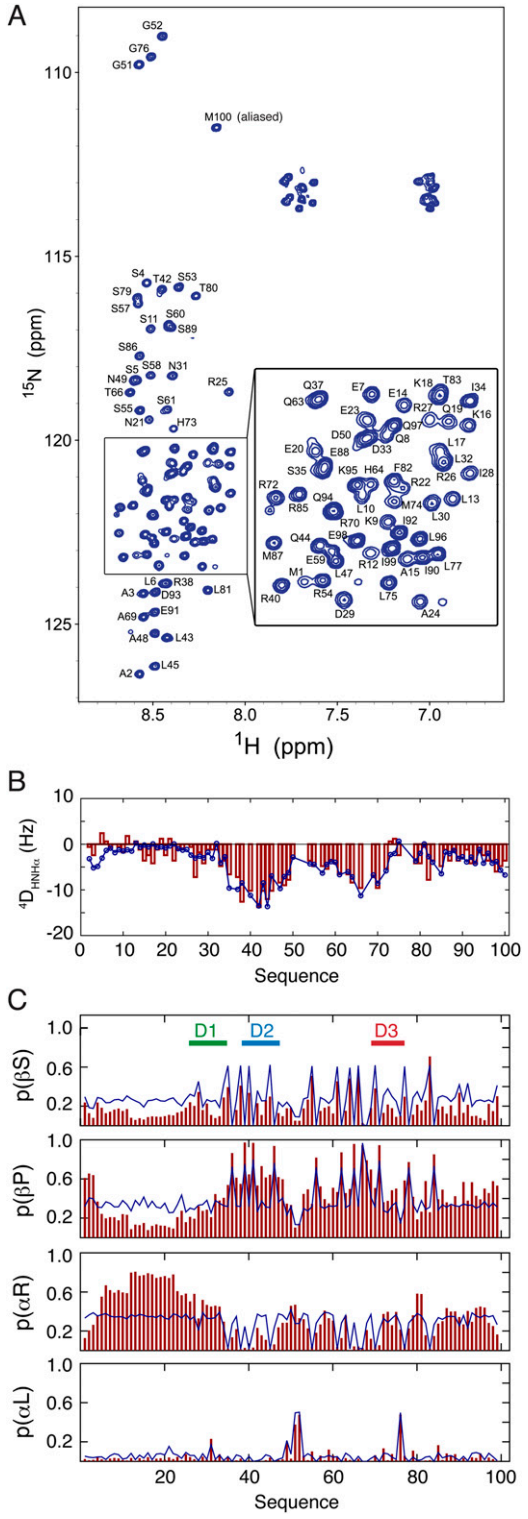

Fig. S2. Characterization of the regulatory domain of MKK7. (*A*) Assigned ^{1}H-^{15}N HSQC spectrum of the regulatory domain of MKK7 at 5 °C and pH 7.0. (*B*) Reproduction of independent (passive) experimental data by the ASTEROIDS ensembles of MKK7 derived on the basis of ^{13}Cα, ^{13}Cβ, ^{13}C′, ^{15}N, and ^{1}H^{N} chemical shifts and $^{1}D_{NH}$, $^{1}D_{C\alpha H\alpha}$, and $^{1}D_{C\alpha C'}$ RDCs. Experimental $^{4}D_{HNH\alpha}$ RDCs are shown in red, whereas back-calculated RDCs from the derived ASTEROIDS ensembles are shown in blue. (*C*) Conformational sampling of the regulatory domain of MKK7 derived from five ASTEROIDS ensembles selected against experimental chemical shifts and RDCs. The sampling is shown in four different regions of Ramachandran space defined as: αL {$\phi > 0°$, $-180° < \psi < 180°$}; αR {$\phi < 0°$, $-120° < \psi < 50°$}; βP {$-100° < \phi < 0°$, $\psi > 50°$ or $\psi < -120°$}; βS {$-180° < \phi < -100°$, $\psi > 50°$ or $\psi < -120°$}. The populations of these quadrants are denoted as p(αL), p(αR), p(βP), and p(βS), respectively. The sampling was averaged over five independent ASTEROIDS runs (red bars). The blue lines correspond to the populations in the statistical coil library.

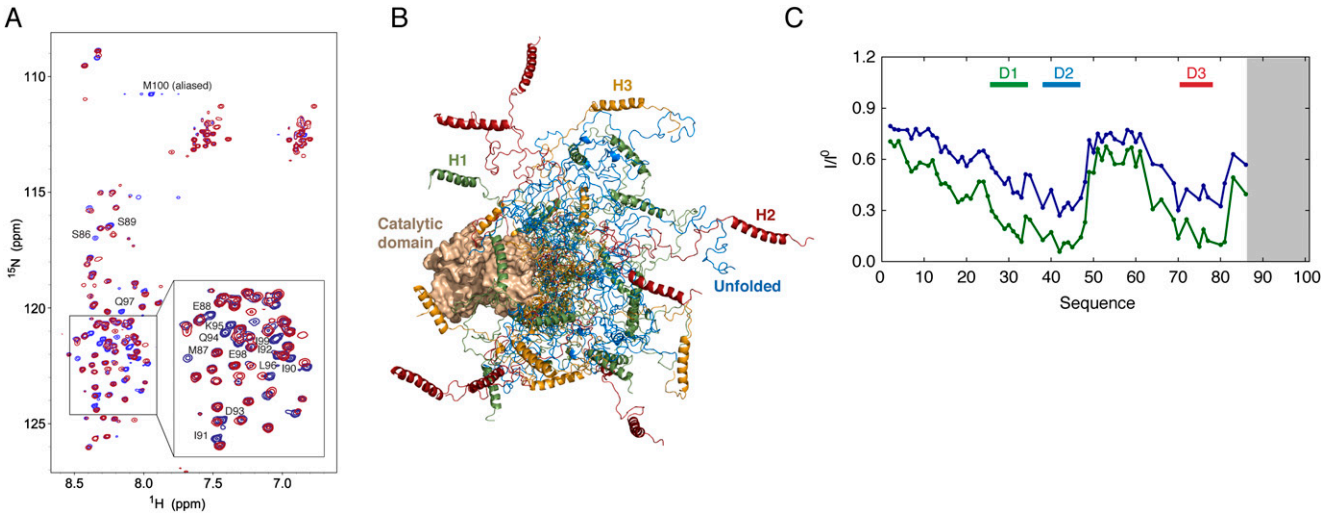

Fig. S3. NMR studies of full-length MKK7. (*A*) Superposition of the ^{1}H-^{15}N HSQC spectrum of full-length MKK7 (red) and the regulatory domain alone (blue) at 25 °C and pH 7.0. Labels indicate resonances that disappear in the context of the full-length protein. Signals from the catalytic domain were not observed in the HSQC spectrum of the full-length kinase due to the slow tumbling of this domain in the presence of the disordered regulatory domain. Resonances corresponding to the residues 86–100 of MKK7 are not observed, probably because of reduced flexibility caused by their proximity to the catalytic domain. (*B*) Model of full-length MKK7. The catalytic domain is shown as a surface representation (beige) (PDB ID code: 2DYL, RIKEN Structural Genomics/Proteomics Initiative), whereas the disordered regulatory domain is represented in four different colors (blue, unfolded; green, helix H1; red, helix H2; yellow, helix H3) corresponding to the conformational equilibrium presented in Fig. 2*C*. The model maps the volume space accessible to the regulatory domain relative to the catalytic domain of MKK7. (*C*) Interaction of JNK1 with full-length MKK7. Intensity profile of the HSQC spectrum of MKK7 with increasing amounts of JNK1: 20% (blue) and 40% (green). NMR signals were observed only for the first 85 residues of MKK7. The intensity ratio I/I^0 is shown, where I is the intensity in the spectrum with a given molar ratio of JNK1, whereas I^0 is the intensity in the spectrum without JNK1.

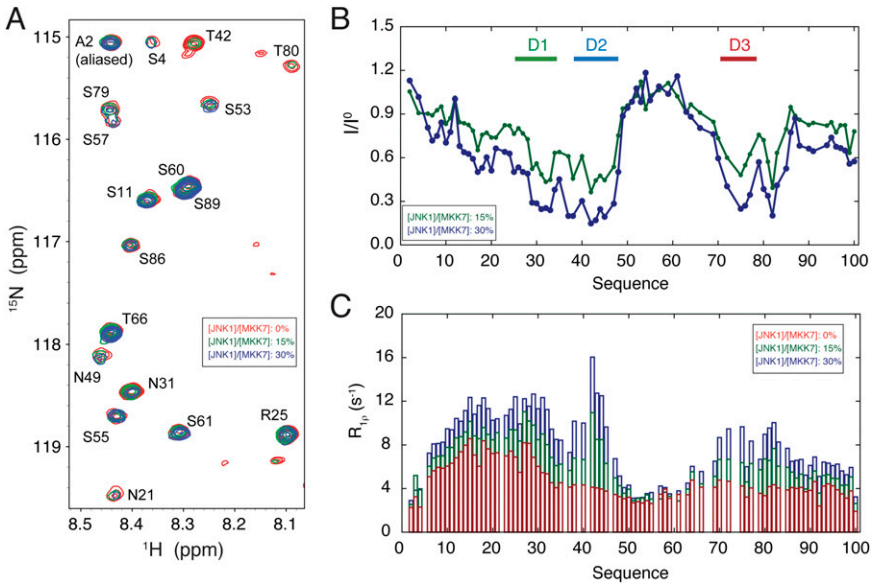

Fig. S4. Interaction of the regulatory domain of MKK7 with JNK1 observed by NMR at 20 °C. (*A*) Region of the ^{1}H-^{15}N HSQC spectra of the regulatory domain of MKK7 in the absence (red) and presence of 15% (green) and 30% (blue) JNK1. Note that some resonances have disappeared from the spectrum because of fast amide proton exchange rates compared with the 5 °C spectra shown in Fig. 4*A*. (*B*) Intensity profile of the regulatory domain with increasing amounts of JNK1: 15% (green) and 30% (blue). (*C*) $R_{1\rho}$ relaxation rates at 850 MHz and 20 °C of the regulatory domain in the absence of JNK1 (red) and presence of increasing amounts of JNK1: 15% (green) and 30% (blue).

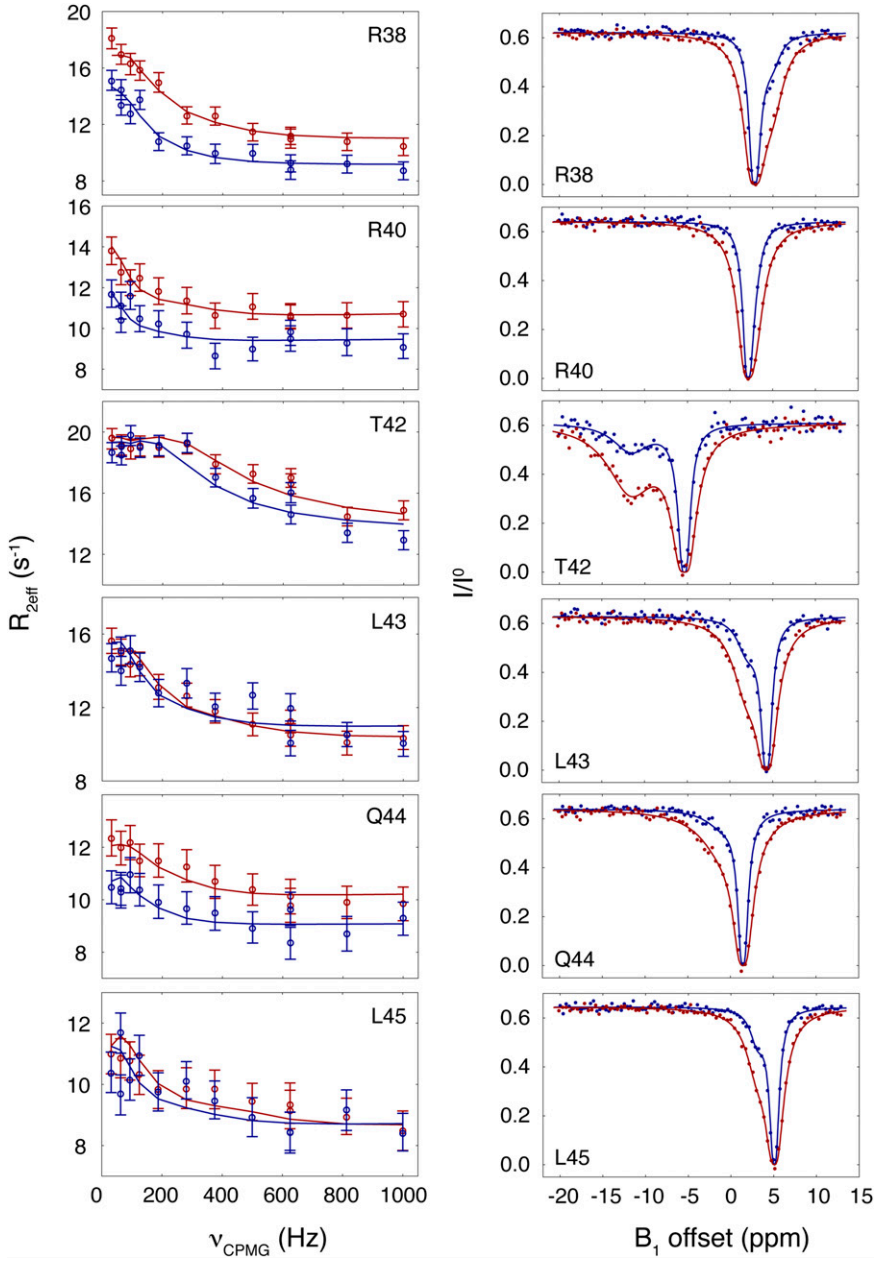

Fig. S5. Relaxation dispersion and CEST profiles of residues within the second docking site of MKK7. The relaxation dispersion experiments (*Left*) were carried out at a ^{1}H frequency of 600 MHz (blue) and 800 MHz (red), whereas the CEST experiments (*Right*) were carried out at ^{15}N B_1 saturating fields of 22 Hz (blue) and 44.5 Hz (red). The dispersion and CEST data were fitted simultaneously for each residue, and the lines correspond to fits according to a two-site exchange model.

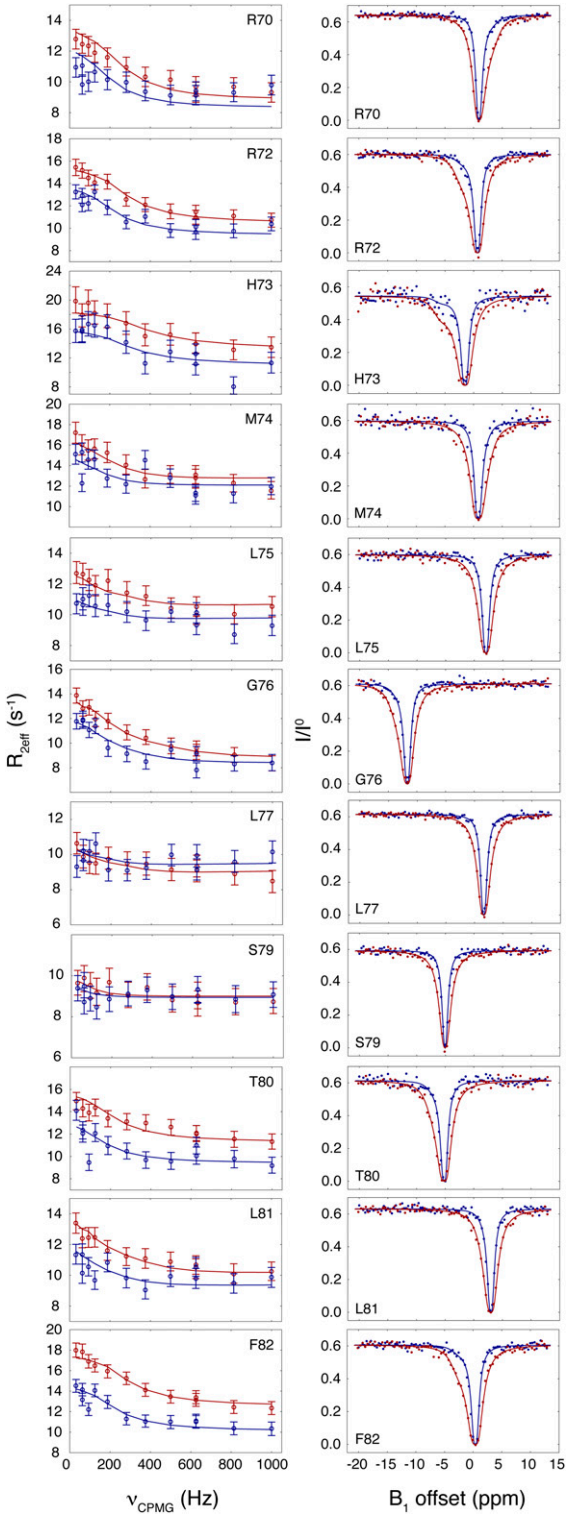

Fig. S6. Relaxation dispersion and CEST profiles of residues within the third docking site of MKK7. The relaxation dispersion experiments (*Left*) were carried out at a ^{1}H frequency of 600 MHz (blue) and 800 MHz (red), whereas the CEST experiments (*Right*) were carried out at ^{15}N B_1 saturating fields of 22 Hz (blue) and 44.5 Hz (red). The dispersion and CEST data were fitted simultaneously for all residues to a single exchange rate and population, whereas the chemical shift changes between the free and bound state of MKK7 were allowed to vary along the sequence. The lines correspond to fits according to a two-site exchange model.

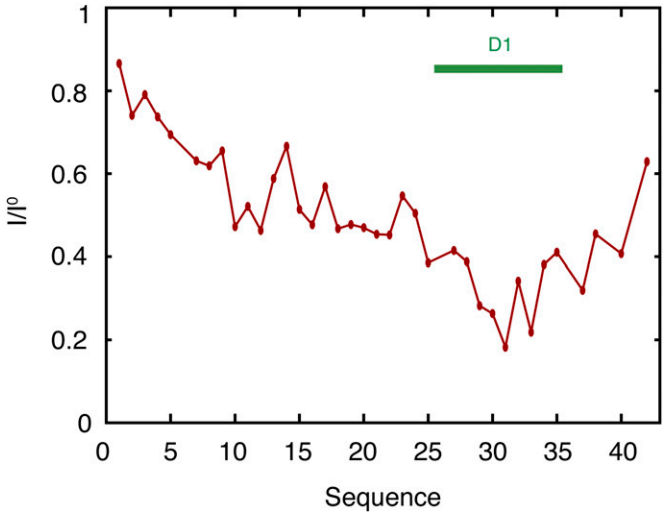

Fig. S7. Interaction of the regulatory domain of MKK7 (residues 1–42) with JNK1 observed by NMR at 5 °C. The intensity profile was calculated as the ratio between the HSQC resonance intensities in the presence of 20% molar ratio of JNK1 (I) and in the absence of JNK1 (I^0).

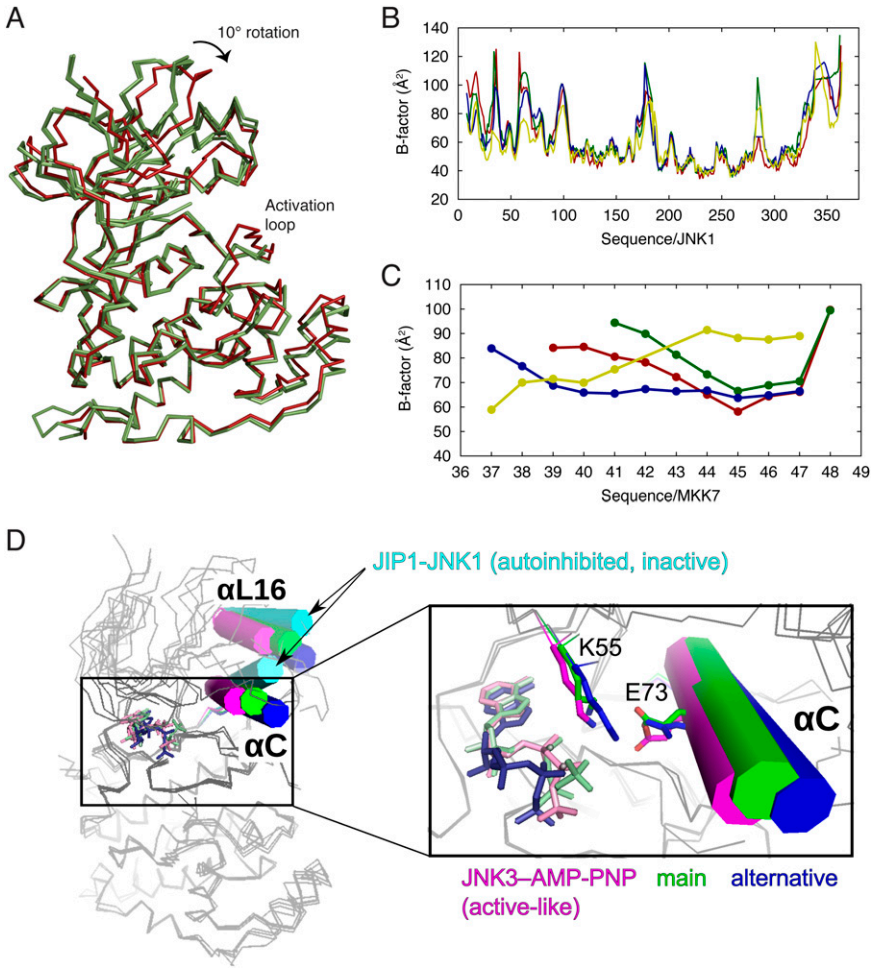

Fig. S8. Analysis of the crystal structures of the JNK1–D2 complex. (*A*) Crystal structure of JNK1 in complex with the D2 docking site peptide showing the superposition of the four JNK1 molecules in the asymmetric unit. The chain D (red) shows a different relative orientation of the N- and C-terminal domains compared with the chains A, B, and C (green). (*B*) B factors (Cα atoms) for JNK1 shown for subunit A (red), subunit B (green), subunit C (blue), and subunit D (yellow). Subunit D corresponds to the alternative conformation of the MKK7 peptide. (*C*) B factors for the D2 peptide of MKK7. (*D*) Comparison of the structures of the JNK1–MKK7D2 complex with previously solved crystal structures. The structure of JNK3 (magenta, PDB ID code 1JNK) in complex with AMP-PNP adopts an active-state conformation (1, 2), whereas the structure of JNK1 in complex with the JIP1 peptide and an inhibitor at the ATP binding pocket (cyan, PDB ID code 1UKH) represents an auto-inhibited conformation that displays a 15° interlobe twist compared with the JNK3 structure (2–4). Both structures of JNK1 that have the D2 peptide bound in the main (green) and alternative conformations (blue) (JNK1-main and JNK1-alternative, respectively) display a tilt of the αC and αL16 helices (cylinders). The JNK1-main conformation is similar to the structure of the active-like JNK3. The position of the AMP-PNP in JNK3 and JNK1-main are overlapping and the catalytic lysine K55 is coordinated between the AMP-PNP and E73 of the αC helix. The αC helix in the JNK1-alternative conformation is further away from the AMP-PNP and the triphosphate moiety of AMP-PNP has moved out of the ATP binding pocket. The JNK1-alternative conformation therefore represents an auto-inhibited conformation in comparison with the more active-like conformation of the JNK1-main structures.

1. Xie X, et al. (1998) Crystal structure of JNK3: A kinase implicated in neuronal apoptosis. *Structure* 6(8):983–991.
2. Laughlin JD, et al. (2012) Structural mechanisms of allostery and autoinhibition in JNK family kinases. *Structure* 20(12):2174–2184.
3. Heo YS, et al. (2004) Structural basis for the selective inhibition of JNK1 by the scaffolding protein JIP1 and SP600125. *EMBO J* 23(11):2185–2195.
4. Ember B, LoGrasso P (2008) Mechanistic characterization for c-jun-N-Terminal Kinase 1alpha1. *Arch Biochem Biophys* 477(2):324–329.

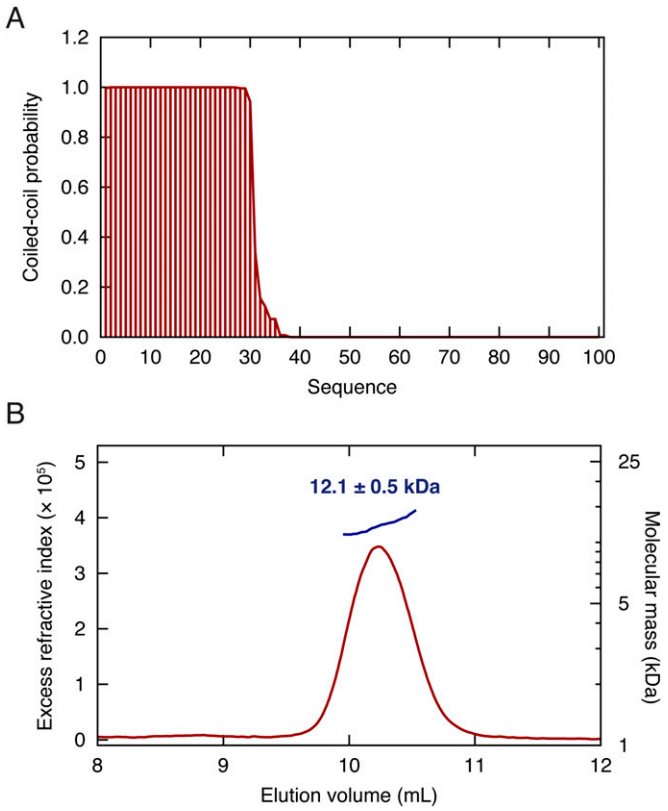

Fig. S9. The regulatory domain of MKK7 predicts to be a coiled-coil, but is monomeric in solution. (*A*) Coiled-coil prediction of the regulatory domain of MKK7 using COILS (1) with a window of 21 residues. The first 30 aa of the domain predict to sample coiled-coil conformations. (*B*) Determination of the molecular mass of the regulatory domain of MKK7 from size exclusion chromatography (SEC) combined with detection by multiangle laser light scattering (MALLS) and refractometry. The red line shows the SEC elution profile as monitored by refractometry (left axis), whereas the blue line shows the molecular mass calculated from light scattering and refractometry data across the elution peak (right axis). The data show that the regulatory domain of MKK7 is monomeric in solution (molecular mass calculated from sequence is 11,458 Da). The protein was injected into the SEC column at a concentration of 28 mg/mL.

1. Lupas A, Van Dyke M, Stock J (1991) Predicting coiled coils from protein sequences. *Science* 252(5009):1162–1164.

Table S1. Data collection and refinement statistics for the complex of JNK1 and the D2 docking site peptide of MKK7

Statistics	PDB 4UX9
Wavelength, Å	0.9
Resolution range, Å	49.21–2.34 (2.424–2.340)
Space group	C 1 2 1
Unit cell	
a, *b*, *c*, Å	108.666, 180.159, 101.144
α, β, γ, °	90.0, 110.3, 90.0
Total reflections	259,709 (20,637)
Unique reflections	75,430 (6,959)
Multiplicity	3.4 (3.0)
Completeness, %	98.42 (91.22)
Mean $I/\sigma(I)$	15.74 (1.53)
Wilson B factor, Å^2	54.67
R_{merge}	0.05315 (0.7338)
R_{meas}	0.06293
$CC_{1/2}$	0.999 (0.576)
R_{work}	0.1912 (0.3219)
R_{free}	0.2375 (0.3605)
No. of nonhydrogen atoms	11,678
Macromolecules	11,189
Water	275
No. of protein residues	1,386
rms deviations	
Bond lengths, Å	0.014
Bond angles, °	1.76
Ramachandran favored, %	97
Ramachandran outliers, %	0
Clash score	2.46
Average B factor, Å^2	65.40
Macromolecules	65.00
Ligand	101.40
Solvent	54.50

Statistics for the highest-resolution shell are shown in parentheses.